Research Article

Facile preparation of high-strength α-$CaSO_4 \cdot 0.5H_2O$ regulated by maleic acid from phosphogypsum: experimental and molecular dynamics simulation studies

Jinfeng Liu[1,2] · Faqin Dong[2] · Hongbin Tan[1,2] · Hongping Zhang[1] · Lei Zhou[2] · Ping He[1] · Lin Zhou[1] · Chenxu Feng[2] · Ruofei Li[2]

Received: 21 April 2020 / Accepted: 20 August 2020 / Published online: 8 September 2020

Abstract
Crystal modifier is a significant factor in preparation of α-hemihydrate gypsum (α-HH) from phosphogypsum (PG). The influence of maleic acid, reaction temperature, time, and solid–liquid ratio on the preparation of high-strength α-HH from PG was systematically studied herein. The optimum condition for α-HH prepared by hydrothermal autoclave method was pH of 4, temperature of 140 °C for 2.0 h with solid–liquid ratio of 4:5. Crystal modifier of maleic acid can effectively regulated the crystal morphology of α-HH. SEM–EDS and FTIR analysis suggested that maleic acid could preferentially absorbed on the top face of α-HH crystals that decreased the growth rate of α-HH along the c-axis, resulting in the morphology of α-HH crystals transformed to hexagonal prisms, and the regulatory mechanism was estimated by molecular dynamics (MD). When maleic acid (0.1%) was added, the obtained α-HH showed aspect ratio of 1.2, and the flexural and compressive strength of the hardened α-HH could reach to 14.79 and 46.24 MPa, respectively. All of these results will help to design long-term effectiveness of phosphogypsum recycling strategies.

Keywords Phosphogypsum recycling · Hydrothermal autoclave method · High-strength α-$CaSO_4 \cdot 0.5H_2O$ · Regulatory mechanism · Molecular simulation

1 Introduction

Phosphogypsum (PG) is a harmful industrial waste produced by the reaction between phosphate rock and sulfuric acid. It is mainly comprised of calcium sulfate dihydrate (DH), which contains various harmful impurities, such as soluble phosphate, fluoride and organic substances of which adhere to the surface of gypsum crystals. And these impurities would replace the DH crystal lattice that limits the applications of PG [1]. In fact, the annual total PG production is assessed to be about 160 million tons worldwide. However, the utilization ratio of PG is only 15.0% [2]. A major portion of PG is still stored for disposal, resulting in severe environment pollution of soil, water and atmosphere [3, 4]. Therefore, the methods of PG recycling have drawn significant attention in more recent years [5, 6]. One of the most key utilization method is to prepare α-hemihydrate gypsum (α-HH) as an important cementitious material with excellent biocompatibility [7, 8] and mechanical strength [9, 10].

Currently, numerous methods have been used for the α-HH production from PG. For example, the salt solution method requires high-concentration salt solutions and washing steps, causing serious corrosion to equipment and secondary pollution [11, 12]. The autoclave method uses lumpy gypsum as pristine material that results in the

✉ Faqin Dong, fqdong@swust.edu.cn | [1]School of Materials Science and Engineering, Southwest University of Science and Technology, Mianyang 621010, China. [2]Key Laboratory of Solid Waste Treatment and Resource Recycle of Ministry of Education, Southwest University of Science and Technology, Mianyang 621010, China.

Table 1 Chemical composition of pristine PG

Components	CaO	SO_3	SiO_2	P_2O_5	Al_2O_3	Fe_2O_3	SrO	TiO_2	K_2O	F	BaO	MgO
Content/%	46.78	40.61	4.78	2.29	1.81	2.26	0.62	0.32	0.18	0.14	0.09	0.08

fluctuation of α-HH quality [13]. In order to simplify the process and obtain high quality crystals, we proposed a new hydrothermal autoclave method without washing steps. This approach is a better way for continuous industrial production compared to the autoclave and salt solution methods. At present, most of α-HH is made from natural gypsum or flue gas desulfurization gypsum, without radioactivity and with fewer harmful impurities [14, 15]. However, few researchers have investigated the preparation of α-HH from PG using hydrothermal autoclave method. In those studies, PG is not used due to the weak radioactivity and complex impurity components [16, 17]. Therefore, preparation of high-strength α-HH from PG would have broad market potential and environmental benefits.

Morphology of α-HH is regarded as one of the primary factors that usually determines its properties and applications [18–20]. For instance, α-HH powder with low aspect ratio has possessed a high flexural and compressive strength [21, 22]. Therefore, the selection of proper crystal modifier is a key way to regulate and control the formation of α-HH crystals with low aspect ratio. Until now, much effort has been devoted to reveal the effects of inorganic salts, surfactants, organic acids (or salt) on the morphology of α-HH [23, 24]. Compared to inorganic salts, organic acids (or salt) can significantly decrease the growth rate of α-HH along the c-axis, and obtain columnar crystal with low aspect ratio [23]. However, the controlling mechanism of modifier to α-HH crystal is still not well understood, and the effect of maleic acid on crystal morphology has not been documented for the process of PG dewatering into α-HH using the hydrothermal autoclave method.

Herein, we introduce hydrothermal autoclave method to prepare α-HH with short hexagonal prisms form PG. Maleic acid was used as the crystal modifier, the effects of reaction time, temperature, and solid–liquid ratio, and crystal modifier on the preparation of high-strength α-HH crystals were systematically investigated. Then MD simulation revealed the regulatory mechanism of the influence of maleic acid on the morphology of α-HH crystals. Additionally, this work also discussed mechanical strength of the hardened α-HH.

2 Materials and methods

2.1 Experimental materials

PG was provided by Sichuan Long Mang Co., Ltd., China. The chemical composition was shown in Table 1. The SEM

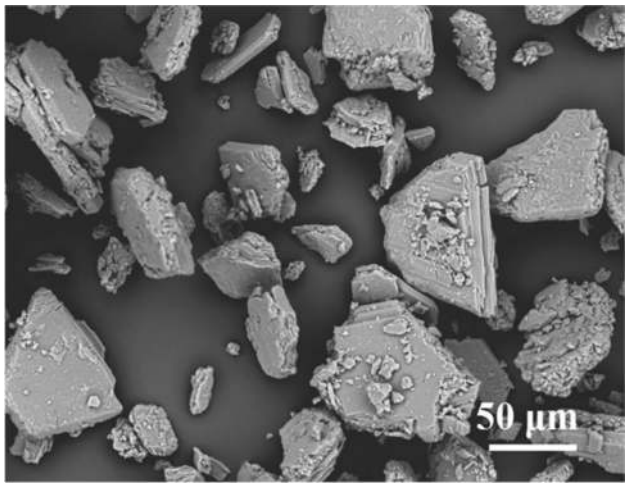

Fig. 1 SEM image of pristine PG

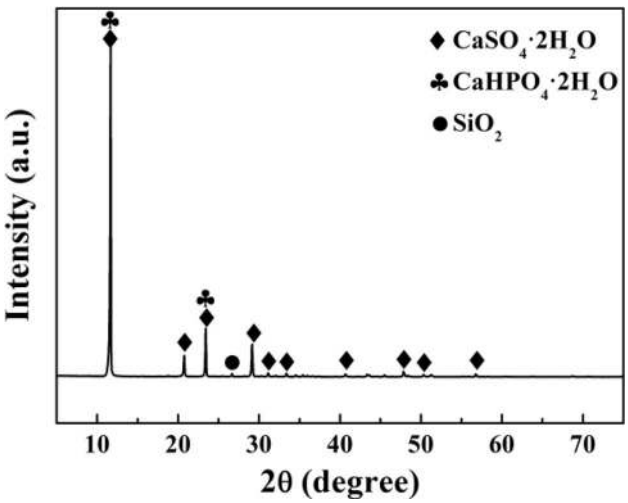

Fig. 2 XRD pattern of pristine PG

morphology of pristine PG was mainly consisted of rhombic shape (Fig. 1). The Fig. 2 showed that the main phase of pristine PG was $CaSO_4{\cdot}2H_2O$ (PDF No. 70-0982). Maleic acid ($C_4H_4O_4$, 99.5%), calcium oxide (CaO, 98%) and sulphuric acid (H_2SO_4, 95–98%) were analytical grade (Chengdu Kelong Chemical Reagent Co., Ltd., China).

2.2 Experimental procedure

Firstly, 2.0% CaO was added to pretreat PG for neutralizing soluble phosphorus, fluorine and residual acids. Next, the

crystal modifier of maleic acid was mixed with deionized water, and the PG samples was added to solution according to the solid liquid ratio of 4:5. Then, the samples were transfered in a 50 mL stainless steel autoclave at 140 °C for 2.0 h. Finally, α-HH was immediately filtered and dried at 110 °C for 4.0 h. Finally, under the same conditions, a 20L autoclave was used to prepare α-HH. Finally, the homogeneous slurry was poured into a mold (40 × 40 × 160 mm) and shaped through vibrations. After removing the film, the test piece is stored under standard conditions for 24 h, and then dried in an oven at 40 ± 1 °C to a constant weight, and then the test piece is cooled to room temperature under the test conditions.

2.3 Characterization methods

X-ray fluorescence spectrometer (XRF, Axios-Poly, PANalytical, Netherlands) was employed to measure the chemical composition of PG. The sample morphology was examined using a scanning electron microscope (SEM, TM-1000, Hitachi, Japan). The sample structure was investigated by an X-ray diffraction spectrometer (XRD, X'pert PRO, PANalytical, Netherlands) using Cu Kα radiation (k = 1.54178Å). The interaction between the α-HH crystal surfaces and malic acid was analyzed using Fourier transform infrared spectrometer (FTIR, Nicolet-5700c, Nigaoli, America). An energy dispersive spectrometer (EDS, IE450X-Max80, Oxford, UK) was used to characterize the presence of chemical element composition. The standard consistency and mechanical strength of α-HH prepared were tested according to the Chinese standard JC/T 2038-2010 by the cement mortar flexural and compressive testing machine (TYE-6A.)

2.4 Simulation

MD simulations were carried out with the materials modeling software package Materials Studio 6.0 (Accelrys Software Inc., San Diego, 2011). COMPASS (condensed-phase optimized molecular potentials for atomistic simulation studies) force fields were used during the whole simulations. Monoclinic crystalline α-HH with the space group of I121 was used here. The unit cell parameters are as follows: a = 12.0317 Å, b = 6.9269 Å, c = 12.6712 Å, β = 90.270°, and Z = 12 [25].

The pure crystal morphology of the α-HH was calculated by the attachment energy (AE) method [26]. As shown in Fig. 3, There are four dominant crystal faces predicted: (002), (110), (200) and (1$\bar{1}$0), as predicted in the previous works [29, 30]. These crystal faces were taken into account in the following modeling. The (002), (200), (110) and (1$\bar{1}$0) faces were cleaved to a fractional depth of 3 and extended to 3 × 4, 3 × 3, 3 × 3, and 3 × 3 unit cells to form a supercell, respectively. A 50 Å vacuum slab was added onto each crystal face to avoid the periodic interactions.

3 ns MD simulations with time step of 1 fs were carried out on each A/B interaction system, NVT ensemble was used and the nose method was used to control temperature [27, 31]. For the potential energy calculations, the electrostatic force was computed by an atom-based summation method with a calculation accuracy of 1×10^{-5} kcal/mol, and the Van Der Walls was computed by the Ewald summation method with a cut off distance of 12.5 Å. The binding energy between the maleic acid and the α-HH surface can be calculated using the following formula:

$$E_{binding} = \left(E_{maleic\ acid} + E_{\alpha-HH}\right) - E_{total}$$

in which *E*total is the total energy of the maleic acid with α-HH system; $E_{\text{maleic acid}}$ is the energy of the maleic acid surface without the α-HH, and $E_{\alpha\text{-HH}}$ is the energy of the α-HH without the maleic acid surface [27, 29].

3 Results and discussion

3.1 Effects of reaction temperature and time on phase transformation from PG to α-HH

In order to study the effects of reaction temperature and time on phase transformation from PG to α-HH, the complete transformation temperature and time were investigated. As shown in Fig. 4, the phase evolution of samples with different temperatures and times were displayed. The XRD pattern of the sample at 120 °C showed the characteristic diffraction peaks of DH (PDF No. 70-0982). When the reaction temperature reached to 130 °C, the diffraction peaks for α-HH (PDF No. 83-0439) appeared along with the

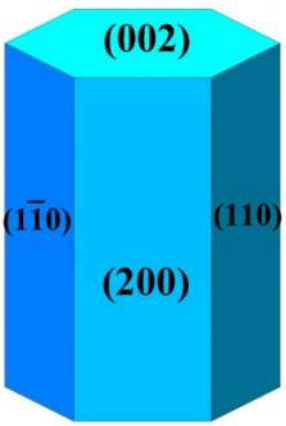

Fig. 3 Theoretical crystal habit of α-HH predicted by the AE method

DH decreasing in intensity, which indicated that the phase transition occurred at 130 °C. When the reaction temperature reached to 140 °C, the XRD pattern presented that α-HH was the only mineral phase based on the diffraction peaks comparison (Fig. 4a). When the reaction time continued for 2.0 h at 140 °C, the sample obtained was α-HH and no DH existed, which demonstrated that DH had been completely converted to α-HH (Fig. 4b).

3.2 Effects of solid–liquid ratio on the morphology of α-HH

The morphology of α-HH crystal has a close relationship with its performance. α-HH crystals with a lower aspect ratio shows better mechanical properties than higher aspect ratio [32]. Solid–liquid ratio is one of the most important parameters that determines α-HH crystal morphology [33]. Thus, SEM morphology (Fig. 5) was used to analyze the effects of solid–liquid ratio on the α-HH crystal morphology. The aspect ratio of crystal gradually decreased with solid–liquid ratio increasing. At low solid–liquid ratio of 4:40 and 4:20 (Fig. 5a, b), bleeding phenomenon of the slurry appeared due to excessive liquid water, leading to the close accumulation of paste. It hindered the heat transfer process of gypsum particles and finally the obtained α-HH crystals had lathy shape and large numbers of small particles. When the solid–liquid ratio reached to 4:5, short prismatic crystal with aspect ratio of 1.5 was obtained (Fig. 5d). In specially, at a high solid–liquid ratio of 4:1, large numbers of holes were seen on the α-HH top face as shown in Fig. 5e. A high solid–liquid ratio was not conducive to crystal growth because the poor water content restrained the mass transfer process of α-HH crystals growing element to crystal surface [19].

3.3 Effects of maleic acid on crystallization

3.3.1 Effects of maleic acid on the morphology of α-HH

As a cementitious material, the mechanical strength of α-HH is an important property of its market value, which depends on the crystal morphology [34]. Crystal modifier is a significant factor in controlling of α-HH crystals morphology. So α-HH crystals prepared with different concentrations of maleic acid were examined to investigate the crystal morphology as presented in Fig. 6. Without the crystal modifier, α-HH samples exhibited lathy shape as a result of their preferential 1-D growth along the c-axis [35, 36] (Fig. 6a). In addition, the distribution of α-HH crystals was uneven with numerous small crystals. When 0.03% maleic acid was present in the reaction system, the aspect ratio declined to 1.4, and the morphology of sample became uniform. However, the top face crystallization of α-HH crystals was incomplete (Fig. 6b). As the maleic acid concentration increased to 0.1%, α-HH crystals remained nearly unchanged in average length. However, the average diameter increased, leading to a decrease in the aspect ratio from 1.4 to 1.2, and all α-HH crystals prepared had hexagonal prisms (Fig. 6d). When the maleic acid concentration reached to 0.5%, the average aspect ratio of α-HH crystals with shorter columns decreased to 0.3 (Fig. 6f). Therefore, the above results indicated that maleic acid is effective in regulating crystal morphology.

The intensity of XRD peaks of corresponding products implies the α-HH crystallinity. Figure 7 showed the XRD patterns of the samples prepared at different concentrations of maleic acid. The peaks of the corresponding samples matched well with α-HH (PDF No. 81-1849). The result indicated that concentration of maleic acid had no

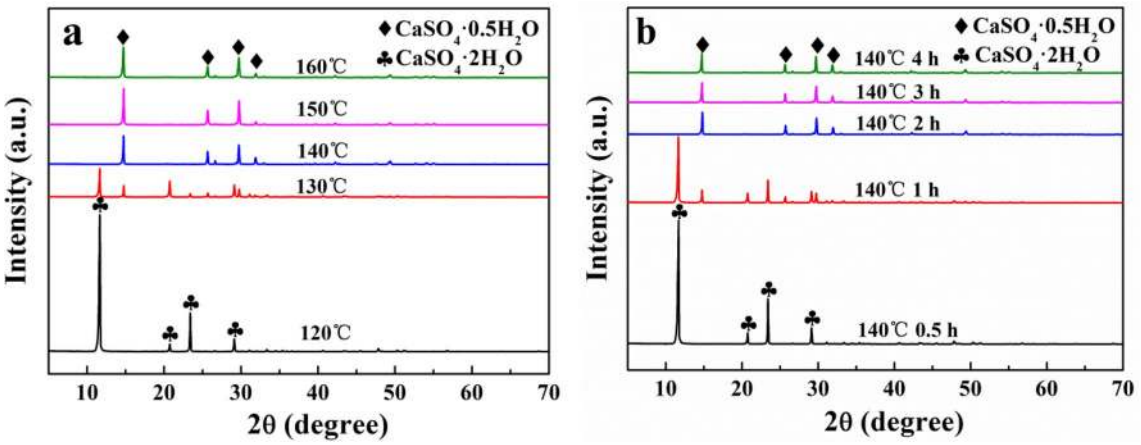

Fig. 4 XRD patterns of the samples prepared at different **a** reaction temperatures **b** and times with 0.05% maleic acid at solid–liquid ratio of 4:5

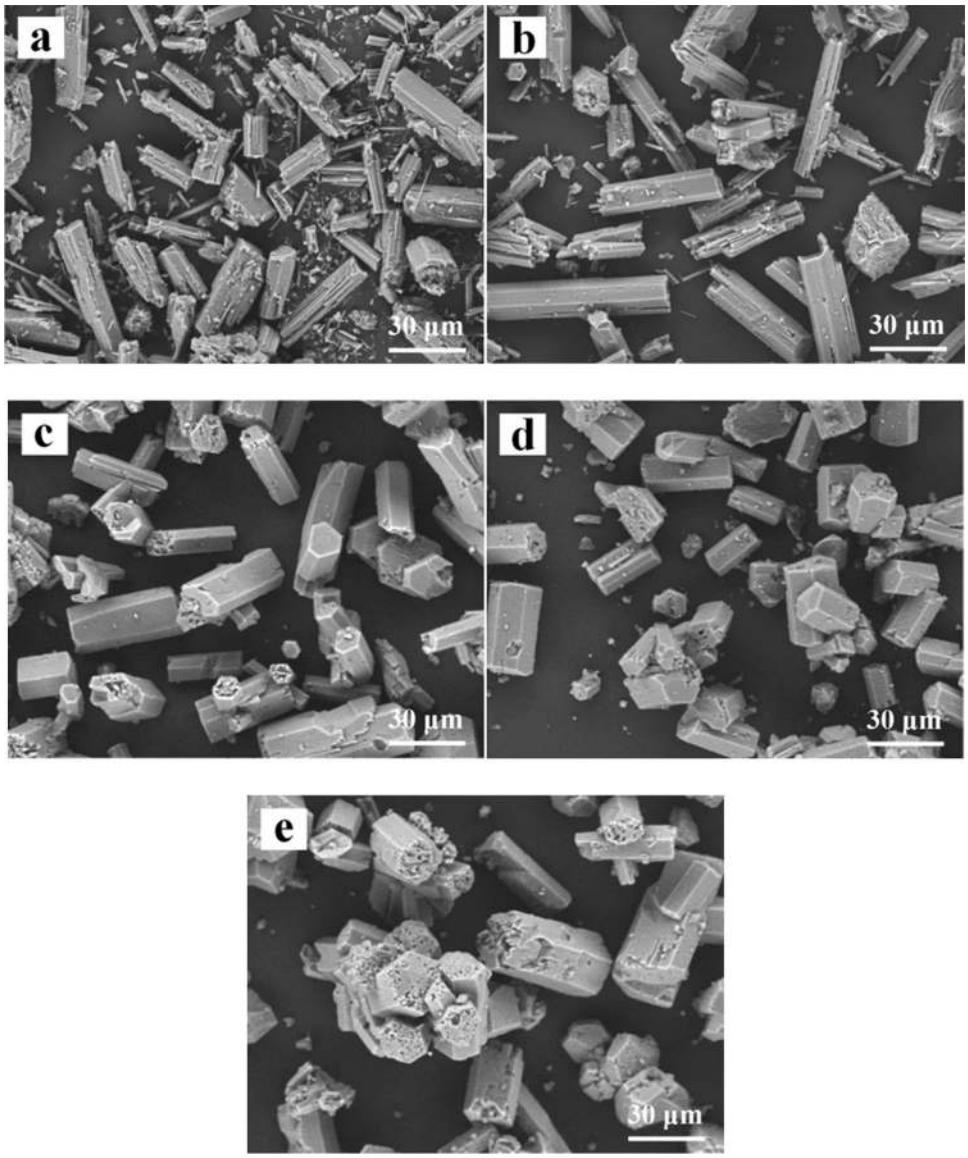

Fig. 5 SEM images of α-HH crystals formed at different solid–liquid ratios with 0.05% maleic acid at 140 °C (**a**: 4:40, **b**: 4:20, **c**: 4:10, **d**: 4:5, **e**: 4:1)

influence on α-HH phase formation. However, with maleic acid concentration increasing, the intensities of (200), (020) and (400) peaks were found to be decreased whereas the intensity of (204) peak was observed to be increased From 1892 to 3410. When the concentration of maleic acid was increased to 0.1%, the intensity of (204) peak reached the highest. It could be inferred that the transformed α-HH crystals had preferred orientation along the (204) face when maleic acid was added to the solution. This result was in good agreement with the SEM morphology showed in Fig. 6, which suggested that the presence of maleic acid may selective adsorption on the active sites of α-HH the crystal surfaces so as to control crystal morphology transformation.

The dominant mechanism of the transformation from DH to α-HH is a process of dissolution–recrystallization [37]. During the reaction process, maleic acid as modifier may tend to absorb on special crystal faces, which would affect the crystal growth. The α-HH top face was mainly consisted of Ca^{2+}, whereas the side face was composed of SO_4^{2-} and Ca^{2+} [23]. The growth rate of the top face with high surface energy along the c-axis was faster than that of side face [12, 15]. Therefore, with maleic acid concentration increasing, the intensities of (200), (020) and (400) peaks decreased gradually. It showed a strong interaction between α-HH crystal faces and maleic acid, affecting the growth rate of different crystal faces. As a result, α-HH crystals morphology presented a typical short prismatic shape.

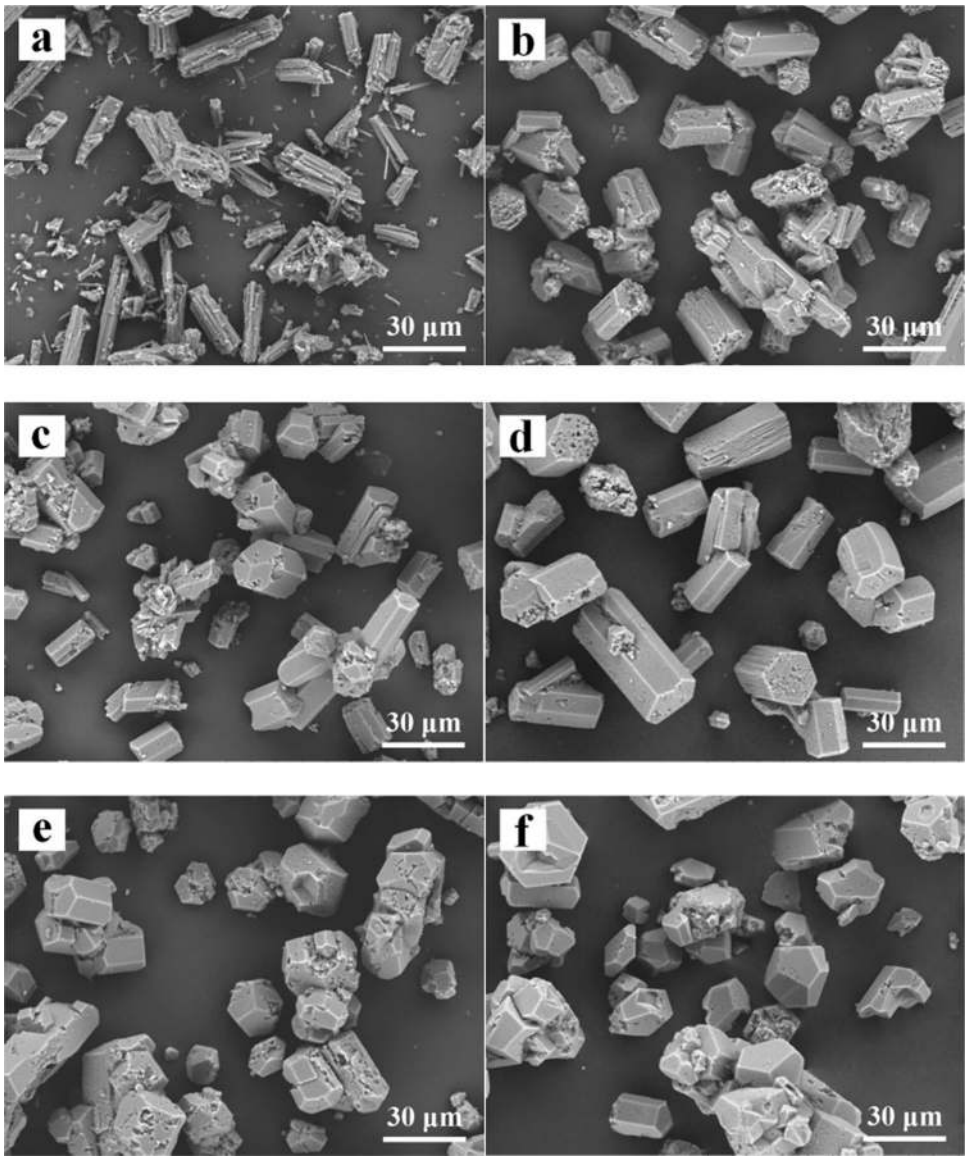

Fig. 6 SEM images of α-HH crystals prepared at different concentrations of maleic acid with solid–liquid ratio of 1:5 at 140 °C (**a**: blank, **b**: 0.03%, **c**: 0.05%, **d**: 0.1%, **e**: 0.3%, **f**: 0.5%)

3.3.2 Effects mechanism of maleic acid on α-HH morphology

Modifier plays a significant role in tuning the morphology of α-HH crystals. Organic acid has been conveyed to be used as a modifier that strongly interactions with α-HH crystal surface are responsible for morphological changes. The interactions are closely reliant to the nature of organic acid and the structure of α-HH. The α-HH crystal lattice is composed of repeating, ionically bonded Ca and SO_4 ions in chains of –Ca–SO_4–Ca–SO_4–, and every two calcium sulfate molecules attaches with one water molecule [24]. The α-HH crystal structure is hexagonal prism that represents the distribution of Ca^{2+} to be denser on the top face and the distribution of SO_4^{2-} denser on the side face so as to the top face positively charged and the side face negatively charged [15, 24]. Therefore, the actual morphology of α-HH grown in the absence of crystal modifiers exhibits needlelike (calcium sulfate hemihydrate whisker) [38]. However, when maleic acid was added to the system, $C_4H_3O_4^-$ selectively absorbed on top face due to strong interaction with Ca^{2+} of α-HH top face. It lowered the surface free energy of top face. Then the crystal tended to grow to minimize the surface area covered by the top face to inhibit α-HH crystal face growth along the c-axis, resulting in the morphology of α-HH crystals transformed to hexagonal prisms with a low aspect ratio as shown in Fig. 8.

To prove the interaction between maleic acid and α-HH crystal surface, FT-IR spectra of α-HH prepared without and with maleic acid were analyzed. As shown in Fig. 9a, in the absence of malic acid, the peaks at 3609.57, 3552.70

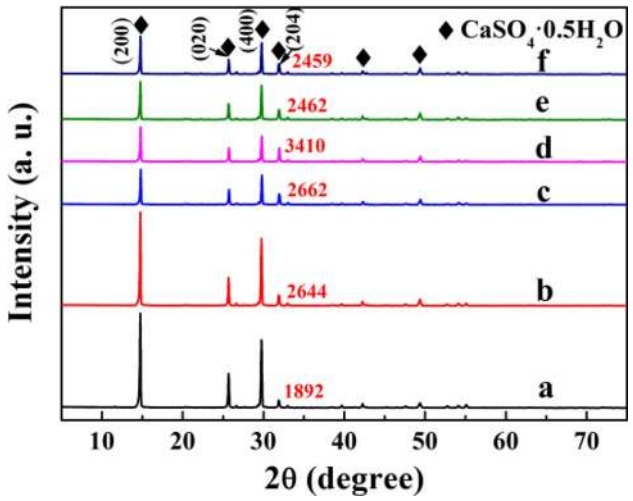

Fig. 7 XRD diffraction patterns of samples prepared at different concentrations of maleic acid with solid–liquid ratio of 1:5 at 140 °C(**a**: blank, **b**: 0.03%, **c**: 0.05%, **d**: 0.1%, **e**: 0.3%, **f**: 0.5%)

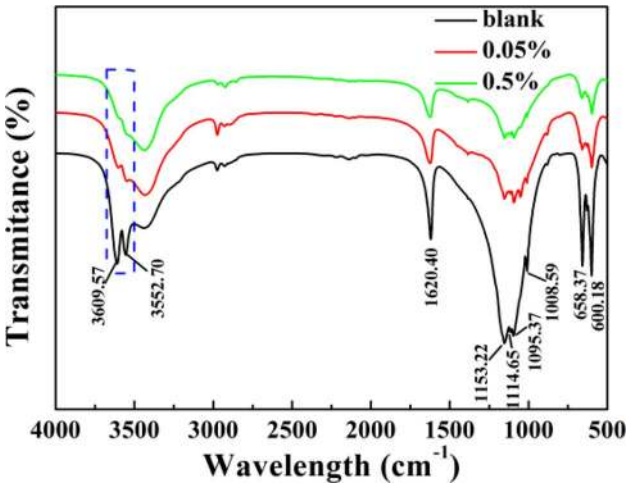

Fig. 9 FT-IR spectra of α-HH prepared with different concentrations of maleic acid

and 1620.40 cm^{-1} could be assigned to O–H vibration of crystal water molecules in the α-HH crystals. The peak at 1008.59 cm^{-1} could be assigned to the distorted symmetric stretching vibration of v_1 SO_4^{2-}. The peaks at 1153.22, 1114.65 and 1095.37 cm^{-1} could be assigned to the asymmetric stretching vibration of v_3 SO_4^{2-}, and the peaks at 658.37 and 600.18 cm^{-1} could be indexed to the v_4 SO_4^{2-} stretching [15, 24]. As shown in spectra b and c, the peaks at 3609.57 and 3552.70 cm^{-1} of O–H vibration gradually become masked with maleic acid concentration increasing. And the α-HH crystal structure showed that water molecules existed in the channels formed by the –Ca–SO_4–Ca–SO_4– chains along the c-axis [36, 39], demonstrating strong interactions between maleic acid and the top face of α-HH crystals.

In order to further confirm the adsorption of maleic acid on the top face of α-HH, EDS analysis was explored to detect the elemental contents on different crystal faces, as shown in Fig. 10 and Table 2. Figure 10 showed that peak of C potentially deriving from maleic acid was found on the top face of α-HH crystals but did not observed on the side face. And Table 2 showed the content of C on the top face and side face was 8.64% and 0.0%, respectively, which confirmed that the effects of maleic acid on the crystal faces were selective. Maleic acid selectively absorbed onto the top face of α-HH crystals.

Additionally, the EDS spectrum also obviously exhibited the increased Ca peak and O peak of side face compared to that of top face. The decreased intensity of Ca peak of top face might be attributed to maleic acid chelating with Ca^{2+} on the top face. The preferential chelation of maleic acid blocked reactive sites of top face and led to slow down the movement rate of Ca^{2+} to the this crystal face, which inhibited the crystal growth along the c-axis. H_2O molecules existed in the chains of the –Ca–SO_4–Ca–SO_4– chains along the c-axis [36, 39], decreased intensity of O peak for top face to side face, which was also confirmed by FT-IR spectra.

Fig. 8 Schematic illustration of the adsorption of maleic acid on the α-HH crystal surfaces

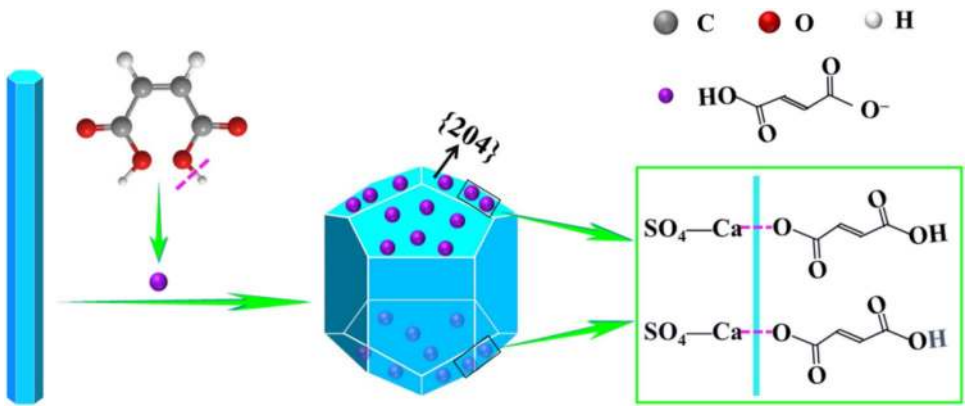

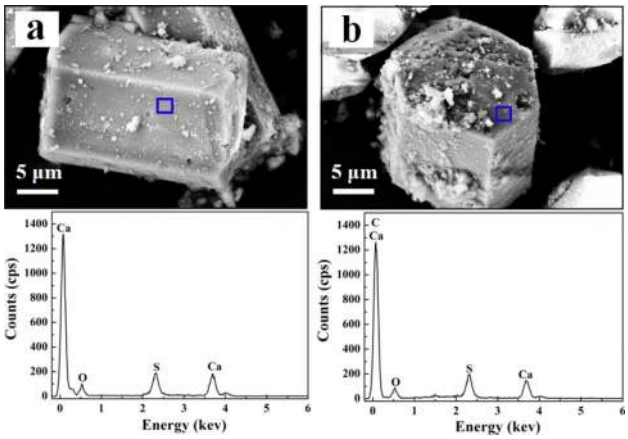

Fig. 10 EDS analyses of α-HH prepared with 0.1% maleic acid (**a**: side face and **b**: top face of the α-HH)

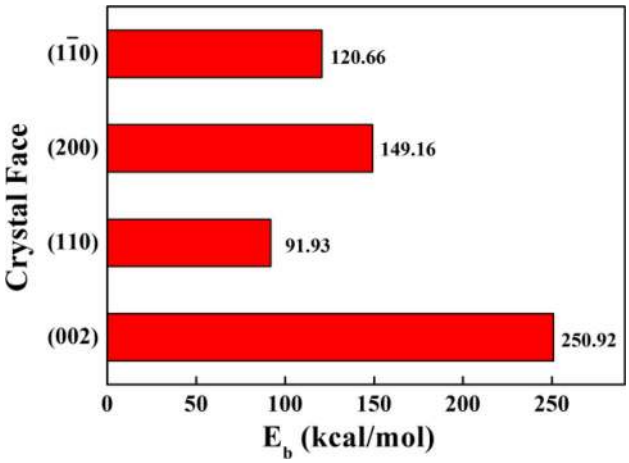

Fig. 11 Binding energy value of different additive/α-HH crystal faces interaction systems

Table 2 Constituents of α-HH prepared with 0.1% maleic acid based on EDS analysis

Elements	Side face of α-CSH		Top face of α-CSH	
	Weight %	Atomic %	Weight %	Atomic %
O K	52.46	71.79	43.03	14.03
S K	16.44	11.23	20.68	57.46
Ca K	31.10	16.98	27.65	13.78
C K	–	–	8.64	14.73
totals	100.00		100.00	

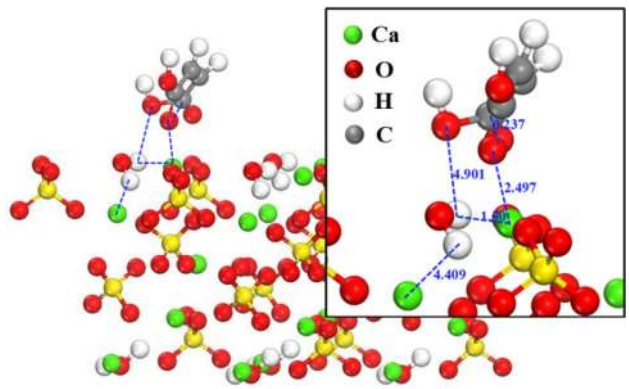

Fig. 12 Equilibrium adsorption configurations of the additive on the (002) face (the blue dash lines denote the distance between atoms)

3.4 Effect mechanism of maleic acid on α-HH by MD simulation

Based on these results above, it was presumed that the inhibition of maleic acid on the α-HH crystal growth was ascribed to the preferential adsorption onto the α-HH top face. When maleic acid was added to the solution, it was primarily adsorbed onto the top face to inhibit the crystal growth along the c-axis. The slower growth rate for the top face led to a sharp decline of the α-HH crystal length. In order to illuminate the adsorption mechanism, the interaction energy of malic acid on different crystal faces was evaluated and analyzed by MD simulation.

The binding energy of (002) face had much larger than the others by comparing the binding energies of maleic acid on the different α-HH crystal faces (Fig. 11), indicating maleic acid preferentially adsorbed on the (002) face. The results showed the different behavior of maleic acid on α-HH crystal faces and it was served as a qualitative indicator to understand the inhibitive effects of maleic acid on crystal growth. The negative values of all the interaction energies indicated that maleic acid could be absorbed on anyone of the crystal faces [27, 28] In addition, the MD result was shown as an example in Fig. 12. The COO^- in maleic acid were negatively charged and would preferentially adsorb on the (002) top face where the Ca atoms were exposed. Therefore, maleic acid inhibited the growth along c-axial, which was in good agreement with the above results of the experimental measurements.

3.5 Effects of maleic acid on mechanical strength of α-HH

Mechanical strength is one important property which determines the quality of α-HH [7, 20]. When α-HH was added to water, α-HH hydrated into DH crystals which generated the mechanical strength. Table 3 showed mechanical strengths of paste prepared from α-HH with 0.1% maleic acid by hydrothermal autoclave method. Without crystal modifier, the 2 h and 3 d bending/compressive strengths of α-HH crystals were 1.79/4.51 MPa

Table 3 Mechanical strength of α-HH using 0.1% maleic acid prepared with hydrothermal autoclave method

Samples	Blank	0.1% maleic acid
2 h blending strength (MPa)	1.79	5.83
2 h compressive strength (MPa)	4.51	17.16
3 d blending strength (MPa)	3.22	14.79
3 d compressive strength (MPa)	8.34	46.24

and 3.22/8.34 MPa, respectively. For α-HH prepared with 0.1% maleic acid, the 2 h and 3 d bending/compressive strengths were 5.83/17.16 MPa and 14.79/46.24 MPa, respectively. The mechanical strength of α-HH was excellent compared to bending/compressive strengths of α-HH prepared in the modifier-free system, and the performance was superior to that of commercial α-HH [33]. So this product could be widely applied in the field of special binder systems, building materials, ceramics industry, molding, medicine and so on.

The enhancement of mechanical strength was attributed to the hexagonal prisms of α-HH crystals with a low aspect ratio [20, 22], which indicated that maleic acid was an effective modifier to regulate mechanical strength of α-HH. Figure 13 showed the morphology of hydration samples of α-HH prepared without additive and with 0.1% maleic acid. As shown in Fig. 13a, the main morphology of the hydration samples was elongated columnar shape while α-HH crystals were prepared without crystal modifier. The structure of DH crystals was not so compact and exhibited a lot of pores, leading to low mechanical strength. Figure 13b showed the hydration samples of α-HH prepared with 0.1% maleic acid. The DH samples of short columnar crystal formed a compact structure by overlapping and interlocking with each other so that the mechanical strength was much higher than that of Fig. 13a.

4 Conclusions

The α-HH was successfully prepared using maleic acid as a modifier in hydrothermal autoclave system. The optimum condition was at pH 4 and maintained at 140 °C for 2.0 h with solid liquid ratio of 4:5. Maleic acid was competent as a crystal modifier to control the α-HH crystal morphology. As the malic acid concentration increased from 0 to 0.5%, the crystal morphology was changed from a lathy shape to short prismatic one, and the average aspect ratio remarkably decreased to 0.3. MD simulation results also showed that maleic acid preferential adsorption on the top face of α-HH crystals was much stronger than the others, which explained the crystal morphology transformation. In both analysis of MD simulation and the experimental results, malic acid as a crystal modifier could inhibit the growth of α-HH crystals along the c-axis, leading to the formation of hexagonal prism crystals.

The mechanical strength of α-HH was relatively low in the modifier-free system. When the appropriate dosage (0.1%) of crystal modifier (maleic acid) was used, the crystal morphology, mechanical strength, and production rate of α-HH improved significantly. The flexural and compressive strength of α-HH were improved to be 14.79 and 46.24 MPa.

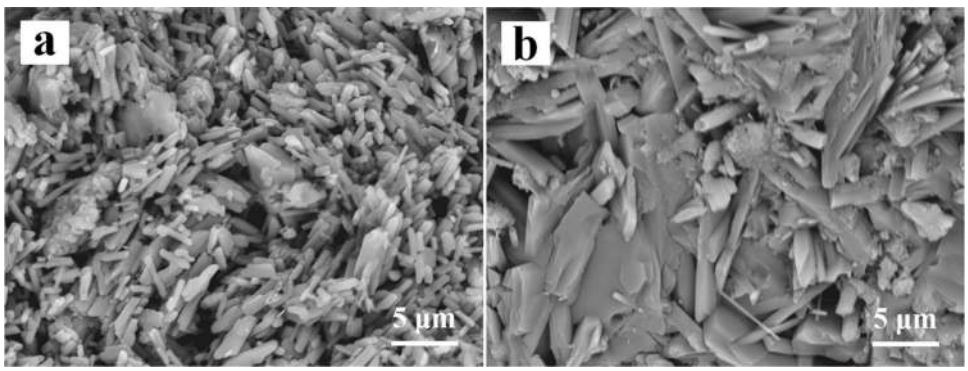

Fig. 13 SEM images of hydration samples of α-HH prepared **a** without additive and **b** with 0.1% maleic acid

Acknowledgements This work was supported by the Sichuan Science and Technology Program [Grant Numbers 2018RZ0040, 2017GZ0401 and 2019YFG0518], State Key Laboratory of Solid Waste Recycling and Energy-Saving Building Materials Program [Grant Numbers SWR-2016-005], Natural Science Foundation of Southwest University of Science and Technology [Grant Numbers 18zx7101].

References

1. Tian T, Yan Y, Hu Z, Xu Y, Chen Y, Shi J (2016) Utilization of original phosphogypsum for the preparation of foam concrete. Constr Build Mater 115:143–152
2. Rashad AM (2017) Phosphogypsum as a construction material. J Clean Prod 166:732–743
3. Tayibi H, Choura M, Lopez FA, Alguacil FJ, Lopez-Delgado A (2009) Environmental impact and management of phosphogypsum. J Environ Manage 90(8):2377–2386
4. Papageorgiou F, Godelitsas A, Mertzimekis TJ, Xanthos S, Voulgaris N, Katsantonis G (2016) Environmental impact of phosphogypsum stockpile in remediated Schistos waste site (Piraeus, Greece) using a combination of gamma-ray spectrometry with geographic information systems. Environ Monit Assess 188(3):133
5. Yang L, Yan Y, Hu Z (2013) Utilization of phosphogypsum for the preparation of non-autoclaved aerated concrete. Constr Build Mater 44:600–606
6. Mechi N, Khiari R, Ammar M, Elaloui E, Belgacem MN (2017) Preparation and application of Tunisian phosphogypsum as fillers in papermaking made from Prunus amygdalus and Tamarisk sp. Powder Technol 312:287–293
7. Li Y, Duan PX, Miao YC, Li Q (2014) Preparation of α high-strength gypsum from FGD gypsum by autoclaved semi-dry process. Adv Mater Res 1051:230–236
8. Garg M, Jain N, Singh M (2009) Development of alpha plaster from phosphogypsum for cementitious binders. Constr Build Mater 23(10):3138–3143
9. Li X, Xu CP, Hou YL, Song JQ, Cui Z, Wang SN, Huang L, Zhou CR, Yu B (2014) A novel resorbable strontium-containing alpha-calcium sulfate hemihydrate bone substitute: a preparation and preliminary study. Biomed Mater 9(4):045010
10. Chen Y, Zhou Y, Yang S, Li JJ, Li X, Ma Y, Hou Y, Jiang N, Xu C, Zhang S, Zeng R, Tu M, Yu B (2016) Novel bone substitute composed of chitosan and strontium-doped alpha-calcium sulfate hemihydrate: Fabrication, characterisation and evaluation of biocompatibility. Mater Sci Eng C Mater Biol Appl 66:84–91
11. Guan B, Kong B, Fu H, Yu J, Jiang G, Yang L (2012) Pilot scale preparation of α-calcium sulfate hemihydrate from FGD gypsum in Ca-K-Mg aqueous solution under atmospheric pressure. Fuel 98:48–54
12. Zhang YQ, Wang D, Zhang LL, Le Y, Wang JX, Chen JF (2017) Facile preparation of α-calcium sulfate hemihydrate with low aspect ratio using high-gravity reactive precipitation combined with a salt solution method at atmospheric pressure. Ind Eng Chem Res 56(47):14053–14059
13. Zürz A, Odler I, Thiemann F, Berghöfer K (2010) Autoclave-free formation of α-hemihydrate gypsum. J Am Ceram Soc 74(5):1117–1124
14. Fu H, Jia C, Chen Q, Cao X, Zhang X (2018) Effect of particle size on the transformation kinetics of flue gas desulfurization gypsum to α-calcium sulfate hemihydrate under hydrothermal conditions. Particuology 40:98–104
15. Guan QJ, Sun W, Hu YH, Yin ZG, Guan CP (2017) Synthesis of α-$CaSO_4 \cdot 0.5H_2O$ from flue gas desulfurization gypsum regulated by $C_4H_4O_4Na_2 \cdot 6H_2O$ and NaCl in glycerol-water solution. RSC Adv 7(44):27807–27815
16. El-Didamony H, Ali MM, Awwad NS, Attallah MF, Fawzy MM (2013) Radiological characterization and treatment of contaminated phosphogypsum waste. Radiochemistry 55(4):454–459
17. Calin MR, Radulescu I, Calin MA (2015) Measurement and evaluation of natural radioactivity in phosphogypsum in industrial areas from Romania. J Radioanal Nucl Chem 304(3):1303–1312
18. Pan Z, Yang G, Lou Y, Xue E, Xu H, Miao X, Liu J, Hu C, Huang Q (2013) Morphology control and self-setting modification of α-calcium sulfate hemihydrate bone cement by addition of ethanol. Int J Appl Ceram Technol 10:E219–E225
19. Jiang G, Wang H, Chen Q, Zhang X, Wu Z, Guan B (2016) Preparation of alpha-calcium sulfate hemihydrate from FGD gypsum in chloride-free $Ca(NO_3)_2$ solution under mild conditions. Fuel 174:235–241
20. Shao D, Zhao B, Zhang H, Wang Z, Shi C, Cao J (2017) Preparation of large-grained α-high strength gypsum with FGD gypsum. Cryst Res Technol 52(7):1700078
21. Huan Z, Chang J (2007) Self-setting properties and in vitro bioactivity of calcium sulfate hemihydrate-tricalcium silicate composite bone cements. Acta Biomater 3(6):952–960
22. Wang P, Lee EJ, Park CS, Yoon BH, Shin DS, Kim HE, Koh YH, Park SH (2008) Calcium sulfate hemihydrate powders with a controlled morphology for use as bone cement. J Am Ceram Soc 91(6):2039–2042
23. Duan Z, Li J, Li T, Zheng S, Han W, Geng Q, Guo H (2017) Influence of crystal modifier on the preparation of α-hemihydrate gypsum from phosphogypsum. Constr Build Mater 133:323–329
24. Kong B, Guan B, Yates MZ, Wu Z (2012) Control of alpha-calcium sulfate hemihydrate morphology using reverse microemulsions. Langmuir ACS J Surf Colloids 28(40):14137–14142
25. Bezou C, Nonat A, Mutin JC, Nørlund Christensen A, Lehmann A (1995) Investigation of the crystal structure of γ-$CaSO_4$, $CaSO_4 \cdot 0.5H_2O$, and $CaSO_4 \cdot 0.6H_2O$ by powder diffraction methods. J Solid State Chem 117:165–176
26. Hartman P, Bennema P (1980) The attachment energy as a habit controlling factor: I. Theoretical considerations. J Cryst Growth 49(1):145–156
27. Fan H, Song X, Liu T, Xu Y, Yu J (2018) Effect of Al^{3+} on crystal morphology and size of calcium sulfate hemihydrate: experimental and molecular dynamics simulation study. J Cryst Growth 495:29–36
28. Li XB, Zhang Q, Ke BL, Wang XC, Li LJ, Li XH, Mao S (2018) Insight into the effect of maleic acid on the preparation of α-hemihydrate gypsum from phosphogypsum in Na_2SO_4 solution. J Cryst Growth 493:34–40
29. Mao X, Song X, Lu G, Sun Y, Xu Y, Yu J (2015) Control of crystal morphology and size of calcium sulfate whiskers in aqueous HCl solutions by additives: experimental and molecular dynamics simulation studies. Ind Eng Chem Res 54(17):4781–4787
30. Mao X, Song X, Lu G, Xu Y, Sun Y, Yu J (2015) Effect of additives on the morphology of calcium sulfate hemihydrate: experimental and molecular dynamics simulation studies. Chem Eng J 278:320–327
31. Schmidt C, Ulrich J (2012) Crystal habit prediction-including the liquid as well as the solid side. Cryst Res Technol 47(6):597–602
32. Li F, Liu J, Yang G, Pan Z, Ni X, Xu H, Huang Q (2013) Effect of pH and succinic acid on the morphology of α-calcium sulfate hemihydrate synthesized by a salt solution method. J Cryst Growth 374:31–36

33. Mi Y, Chen D, He Y, Wang S (2018) Morphology-controlled preparation of α-calcium sulfate hemihydrate from phosphogypsum by semi-liquid method. Cryst Res Technol 53(1):1700162
34. Mi Y, Chen D, Wang S (2018) Utilization of phosphogypsum for the preparation of α-calcium sulfate hemihydrate in chloride-free solution under atmospheric pressure. J Chem Technol Biotechnol 93(8):2371–2379
35. Hou S, Wang J, Wang X, Chen H, Xiang L (2014) Effect of Mg^{2+} on hydrothermal formation of alpha-$CaSO_4 \cdot 0.5H_2O$ whiskers with high aspect ratios. Langmuir ACS J Surf Colloids 30(32):9804–9810
36. Ballirano P, Maras A, Meloni S, Caminiti R (2001) The monoclinic I_2 structure of bassanite, calcium sulphate hemihydrate ($CaSO_4 \cdot 0.5H_2O$). Eur J Mineral 13(5):985–993
37. Guan B, Shen Z, Wu Z, Yang L, Ma X (2008) Effect of pH on the preparation of α-calcium sulfate hemihydrate from FGD gypsum with the hydrothermal method. J Am Ceram Soc 91(12):3835–3840
38. Tang Y, Gao J (2017) Investigation of the effects of sodium dicarboxylates on the crystal habit of calcium sulfate alpha-hemihydrate. Langmuir ACS J Surf Colloids 33(38):9637–9644
39. Freyer D, Voigt W (2003) Crystallization and phase stability of $CaSO_4$ and $CaSO_4$-based salts. Monatsh Chem 134(5):693–719